Comparison of the Land-Surface Interaction in the ECMWF Reanalysis Model with the 1987 FIFE Data

ALAN K. BETTS

Atmospheric Research, Pittsford, Vermont

PEDRO VITERBO AND ANTON C. M. BELJAARS

ECMWF, Reading, Berkshire, United Kingdom

(Manuscript received 5 February 1997, in final form 8 May 1997)

ABSTRACT

Data from the First ISLSCP (International Satellite Land Surface Climatology Project) Field Experiment for the summer season of 1987 are used to assess the land-surface interaction of the ECMWF reanalysis. In comparison with an earlier study, using the 1992 ECMWF operational model, the land-surface interaction is greatly improved. The bias in the incoming solar radiation has been removed, although there seems to be a small low bias in the incoming longwave, which is significant at night. The four-layer soil moisture model depicts the seasonal cycle well, and the root zone is recharged satisfactorily after major rain events. Consequently, the evaporative fraction (EF) over the season is now generally quite good. There is, however, a low bias in EF in June and high bias in October, which is probably due to the absence of a seasonal cycle in the model vegetation. The evaporative fraction also appears too high in the model just after rainfall. It also appears that the model lacks a realistic seasonal control on the soil heat flux. The surface diurnal thermodynamic cycle has two noticeable errors. The temperature minimum at sunrise is too low, because the surface uncouples too much at night under the stable boundary layer, and the incoming longwave radiation is biased low. There is also an unrealistic diurnal cycle of mixing ratio, q, with too strong a midmorning peak, and too large a fall during the day to a late afternoon minimum that is biased low. These errors in the diurnal cycle of q may feed back on the diurnal cycle of precipitation. The morning peak is partly related to the too-strong inversion at sunrise, which slows the deepening of the boundary layer. The late afternoon minimum of mixing ratio (below that of the model analysis) leads to a positive nudging of soil moisture in the analysis cycle. The model summer mixing ratio has a small high bias of 0.5 g kg^{-1}.

1. Introduction

The European Centre for Medium-Range Weather Forecasts (ECMWF) recently completed its reanalysis project, which used a frozen version of their analysis–forecast system, at a triangular spectral truncation of T-106 with 31 levels in the vertical, to perform data assimilation using past data from 1979 to 1993 (Gibson et al. 1997). The National Centers for Environmental Prediction (NCEP) and the National Center for Atmospheric Research (NCAR) have completed a similar reanalysis project with a current version of the Medium Range Forecast (MRF) model (Kalnay et al. 1996). The Data Assimilation Office at the Goddard Laboratory for Atmospheres is also doing a reanalysis for the time period starting in 1985 (Schubert et al. 1993). The study of climate and climate change is driving the need for these uniformly assimilated datasets. Current archives of gridpoint data commonly used in climate studies are derived from operational numerical weather prediction centers and are the results of production data assimilation suites. In studies of the climate change to date, researchers have had to deal with changes in the model data due both to real atmospheric changes and changes in assimilation procedures. For this reason reanalysis projects were proposed some years ago (Bengtsson and Shukla 1988) to remove changes due to assimilation procedures as much as possible. Since the resulting analyses will be valuable to the scientific research community for years to come, it is useful to document the character of the model data by comparison with actual observations, since the current analysis–forecast procedures are certainly not perfect. In another paper (Betts et al. 1996), the land-surface and boundary layer (BL) components of the NCEP–NCAR reanalysis system were compared with the 1987 First ISLSCP (International Satellite Land Surface Climatology Project) Field Experiment (FIFE) dataset. Here we compare the land-surface fluxes and meteorological variables from the

Corresponding author address: Dr. Alan K. Betts, R.D. #3, Box 3125, Pittsford, VT 05763.
E-mail: akbetts@aol.com

ECMWF reanalysis with the same 1987 FIFE data. In a third paper, we use some of the same FIFE data to explore the land-surface errors in two versions of the NCEP regional Eta Model (Betts et al. 1997).

The ECMWF reanalysis has a 6-h analysis cycle, and from every analysis a 6-h short-term forecast is run. The meteorological state variables at the surface are archived at 3 and 6 h from these forecasts, as well as the surface fluxes averaged for the 0–3- and 3–6-h forecasts. Consequently, we can compare at a 3-h time resolution the surface meteorological parameters and surface energy budget of the closest grid point (see section 2c) in the T-106 reanalysis with site-averaged data from 1987 (Betts and Ball 1998) from the FIFE site in the Konza prairie, south of Manhattan, Kansas. During FIFE, an extensive series of surface meteorological observations, data from radiosondes, and surface energy budget measurements were collected during the 1987 summer growing season (Sellers et al. 1988; Sellers et al. 1992). The FIFE observations were made on a 15 km $\times$ 15 km site. Betts et al. (1993) averaged the surface meteorological and flux data to give a single time series representative of the FIFE site for the time period May–October 1987 and used this dataset to identify errors in the ECMWF land-surface and BL formulations. Subsequently, this and other datasets were used to develop improved parameterizations for that model (Viterbo and Beljaars 1995), which were incorporated in the operational ECMWF model, which was used in the reanalysis project. In this paper, we are taking the data from the reanalysis from the grid point near FIFE and asking how the full reanalysis model, run for a 15-yr period, is able to reproduce the FIFE site-average time series in 1987, which we have since updated in Betts and Ball (1998).

The model representation of the diurnal and seasonal cycle is not surprisingly much better than in our earlier study (Betts et al. 1993), but once again the comparison with data identifies aspects of the model parameterizations that need further development. As we pointed out in Betts et al. (1996), it is important to realize that we are using an average time series for a 15 km $\times$ 15 km domain in Kansas (centered near 39°N, 96.5°W) to identify systematic errors in a global model with a considerably larger effective grid resolution of order 100 km. The center of the ECMWF grid box we are using for comparison is at 38.68°N, 96.25°W, about 40 km southeast of the FIFE site. There are several reasons why the comparison is meaningful. For the summer of 1987, conditions over the FIFE grassland site were relatively homogeneous, so that simple averaging of the data gave a representative mean. The disparity of scale is partly offset by the fact that the diurnal cycle over land integrates over considerable advection distances (of order 100–200 km). Over the central United States, the rawinsonde network is sufficiently dense to define the synoptic-scale fields down to almost the resolution of the global model. On this scale the fields are smoothly varying, so that even if we had used an adjacent grid point from the global model, we would probably have reached similar conclusions about the performance of the global model, because the climatological gradient in summer at this location in Kansas is small (about 0.5 g kg^{-1} in mixing ratio per degree of latitude). Although the global reanalysis uses the upper-air observations and some surface synoptic data, the diurnal cycle of temperature and humidity and the surface fluxes over land away from the analysis times are calculated from the model radiation, cloud, and land-surface parameterizations. By studying a range of different conditions over both the seasonal cycle and the diurnal cycle for days with and without rainfall, we will look not for exact detailed agreement between model and observations, but for indications of systematic bias, situations where the model parameterizations do not represent the data in a realistic way. This both gives the user a sense of the quality of the land surface–atmosphere interaction in this reanalysis, as well as indicates directions for further model improvements. Many of our conclusions are relevant to the ECMWF operational model during the summers of 1995 and 1996, which used the same land-surface model as the reanalysis but with the higher T-213 horizontal resolution. More recent changes to the model, which reduce some of the errors discussed in this paper, are reviewed in section 2b.

2. Data and model description

a. FIFE data products used

Both the raw data and most of our averaged time series are available on CD-ROM (Strebel et al. 1994). The details of the production of our initial average data are in the appendix of Betts et al. (1993). The editing of the raw data involved both the use of simple range filters and extensive manual editing of bad data. There were data from up to 10 surface portable automated meteorological stations (labeled AMS in the figures) in each 30-min average. Since the publication of Strebel et al. (1994), this averaged meteorological time series has been extended to November 1989 (Betts and Ball 1995, 1998), and we use here the average time series from May to October 1987. We also reprocessed the surface flux data (labeled FLUX data in the figures) from the surface sites and generated a site flux average for the whole summer period from 25 May to 16 October 1987 (Betts and Ball 1998). This supersedes the flux averages used in our earlier papers (Betts et al. 1993; Betts et al. 1996; Betts et al. 1997). The number of stations in this flux average varies from as many as 17 during the four intensive field campaigns (IFCs), to as few as 4–6 during periods between IFCs.

b. The ECMWF reanalysis model

The reanalysis model is similar to the model used in operations from April 1995 to August 1996. It has 31

vertical levels, and for the reanalysis it was run at the reduced horizontal spectral resolution of T-106 (the operational model runs at T-213). This model includes (i) the land-surface scheme of Viterbo and Beljaars (1995) with the BL modifications described on Beljaars et al. (1996), introduced operationally in August 1993; (ii) the soil moisture initialization procedure (Viterbo and Courtier 1995) introduced in December 1994; and (iii) the prognostic cloud scheme (Tiedtke 1993) and subgrid-scale orography scheme (Lott and Miller 1997) introduced operationally in April 1995. The adiabatic part of the model, using a fully 3D semi-Lagrangian advection scheme, is described in Richie et al. (1995). The vertical levels are defined by hybrid vertical coordinates (Simmons and Strüfing 1981) with between three and eight levels in the boundary layer at approximately 33, 150, 360, 640, 970, 1360, 1800, and 2290 m above the surface. The other important physics components are the radiation scheme by Morcrette (1990) and the mass-flux convection scheme by Tiedtke (1989). As of 1 February 1993, a low-resolution climatological distribution of four kinds of aerosols, namely, continental-desert, maritime, urban, and stratospheric background, with shortwave and longwave effects as described in Tanre et al. (1984) was reactivated in the ECMWF model.

The present (May 1997) operational ECMWF model physics includes two further changes: (i) a treatment of the thermal effects of soil water freezing and modifications to the heat transfer in the stable regime (Viterbo et al. 1997), introduced in September 1996 to alleviate the cold bias in stable conditions; and (ii) modifications to the albedo of the boreal forest in the presence of snow were introduced in December 1996. The first change greatly reduced (in the present operational model) the nighttime cold bias and the somewhat reduced morning bias in humidity that are reported in this paper. We shall briefly show the impact of this new stable boundary layer scheme in section 4c.

c. The concept of the closest grid point

There are several reasons why the notion of a closest grid point is relevant, even for the ECMWF spectral model. (i) The data assimilation used in the reanalysis scheme (optimal interpolation) is performed in gridpoint space. (ii) All the physics computations, including the subsurface transfer of heat and water, take place in gridpoint space. (iii) Advection takes place in gridpoint space, because a semi-Lagrangian scheme is applied. As a result, all computations relevant to the prognostic equation for water vapor are done in gridpoint space. For the purposes of archiving and forward time propagation of the model variables, the spectral space is used, with the exception of humidity. In addition, terms treated implicitly in the dynamics equations (e.g., Coriolis acceleration) are dealt with in spectral space. It is worth mentioning that the Gaussian grid spacing (~112 km) is finer than the smallest scale resolved in spectral space, which is of the order of 200 km (the half-wavelength of the shortest resolved wave at T-106). To the extent that a part of the spatial gradients are represented in spectral space (since all variables, except for humidity, are stored in spectral space), the smallest advection scale represented in the model forecast or analysis data is of the order of 200 km.

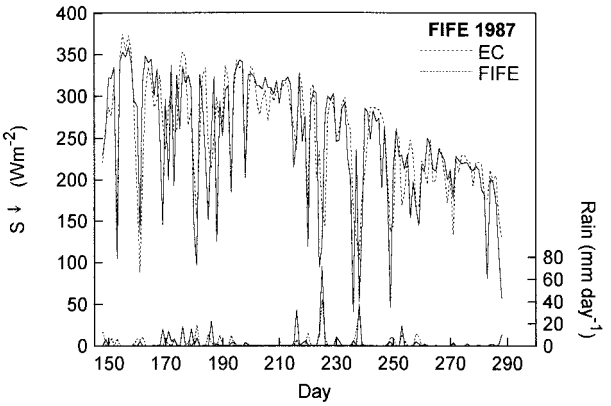

FIG. 1. Comparison of 24-h average incoming solar radiation (S↓) for EC reanalysis and FIFE-1987 FLUX site average. The 24-h precipitation (model and observed) is shown below with the scale on the right.

3. Seasonal comparison with the FIFE data

a. Radiation fluxes and ground flux

We first compare the surface fluxes in the European Centre (EC) reanalysis model with the FIFE-site average. Figure 1 shows the 24-h average of the incoming solar radiation comparison. The agreement is much better than in Betts et al. (1993), showing that modifications to the shortwave radiation scheme (J. J. Morcrette 1996, personal communication), including the reintroduction of aerosols and the addition of the prognostic cloud scheme (Tiedtke 1993), have corrected the high bias in incoming solar seen in our earlier study. The data are an average of the FLUX station data. On average, the drop in downwelling solar in the model with rain events is also close to that observed. The daily precipitation (both model and observed) is shown below with a right-hand scale. The model albedo at this grid point is a fixed 16.5%, slightly lower than the 18%–19% observed.

The surface energy budget is given by

$$R_n + \mathrm{SH} + \mathrm{LH} + G = 0, \qquad (1)$$

where R_n is net radiation, SH and LH are the surface sensible and latent heat fluxes, and G is the ground heat flux. Our sign convention is that fluxes toward the surface are positive, so that on a typical sunny day, R_n is positive while SH, LH, and G are negative. Figure 2 compares the 24-h average surface net radiation R_n and ground heat flux G. We show two observed net radiation curves, one the average of the AMS stations (dashed)

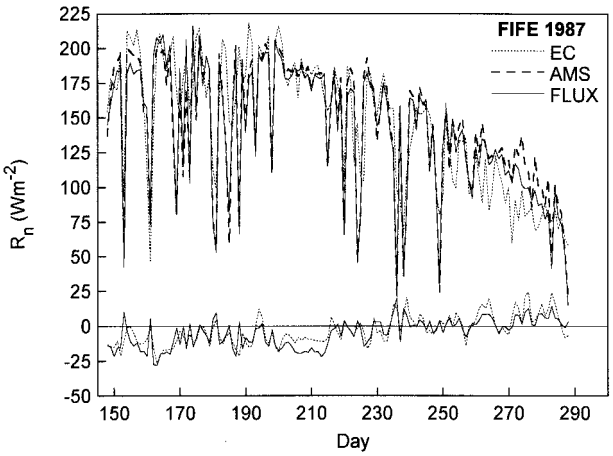

FIG. 2. As in Fig. 1 but for net radiation R_n, including AMS and FLUX site average and ground heat flux, G.

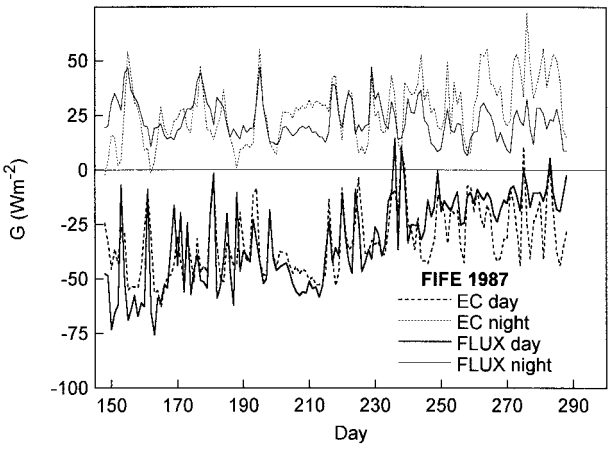

FIG. 4. Ground heat flux comparison for daytime (1200–2400 UTC) and nighttime (0000–1200 UTC) averages.

and the other the average of the FLUX stations (solid), because there were unresolved issues in the calibration of the FIFE net radiometers (Smith et al. 1992a; Smith et al. 1992b). Except in the fall, when the model R_n is lower than both measured estimates, the agreement for the 24-h average is generally good. In the 1200–2400 UTC daytime period, the model has a high bias in R_n in spring and summer (not shown), partly because of its lower albedo. The ground heat flux comparison is the lower pair of curves. In fall again there seems to be some bias, with the model having too large an upward flux, averaged over 24 h.

Figure 3 compares R_n for the 12-h nighttime average (0000–1200 UTC). We again show both AMS and FLUX nighttime averages for the whole summer, and in addition, after day 260 (when the solar flux is negligible for this 12-h period), we show the difference of the longwave fluxes, LW$\downarrow$ − LW$\uparrow$ (short dashes), as measured by two pairs of calibrated pyrgeometers (Smith et al. 1992b). The nighttime EC net outgoing flux is generally higher than observed, and the difference grows in the fall to about 20 W m^{-2}, when it appears to be the model incoming LW flux that is low (not shown). This is the major cause of the fall bias in the 24-h-averaged R_n in Fig. 2.

Figure 4 shows the day (1200–2400 UTC average) and night (0000–1200 UTC) contributions to the ground heat flux. The seasonal trends of model and data show some differences. In the spring, the model G is a little less in magnitude, both day and night than the data, while in the fall, the model ground heat flux is generally larger in amplitude than the data, both day and night. The absolute significance of these differences is harder to assess, as the measurements of G are rather site specific and are likely to be less representative of the large scale than the R_n measurements. When many of the flux stations were moved in 1988, the site mean G changed considerably [at the new sites G/R_n was considerably lower in 1988 than 1987; Betts and Ball (1998)]. However, the difference in seasonal trends is likely to be significant, and it is likely that the EC ground fluxes are biased high in fall.

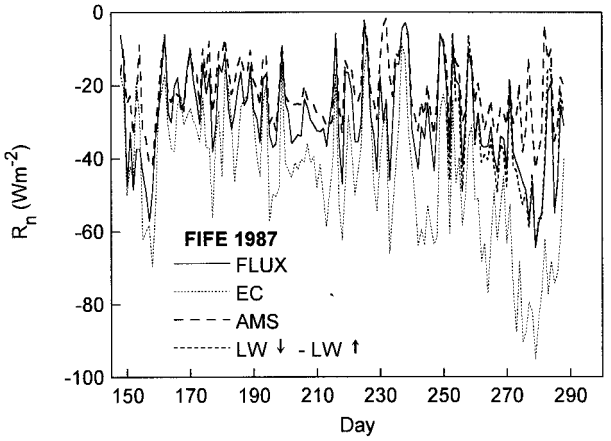

FIG. 3. As in Fig. 2 but for 12-h nighttime R_n (0000–1200 UTC).

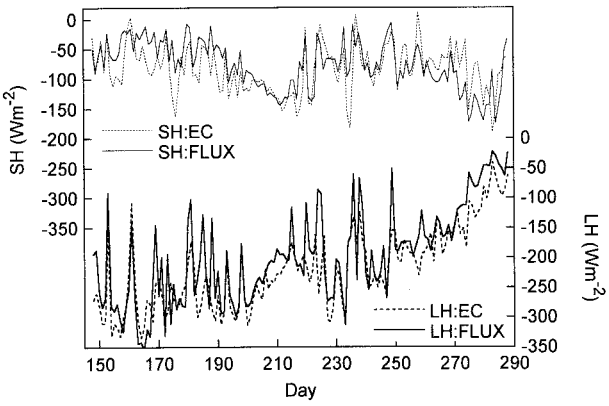

FIG. 5. Comparison of daytime (1200–2400 UTC) latent heat (upper curves) and sensible heat (lower curves).

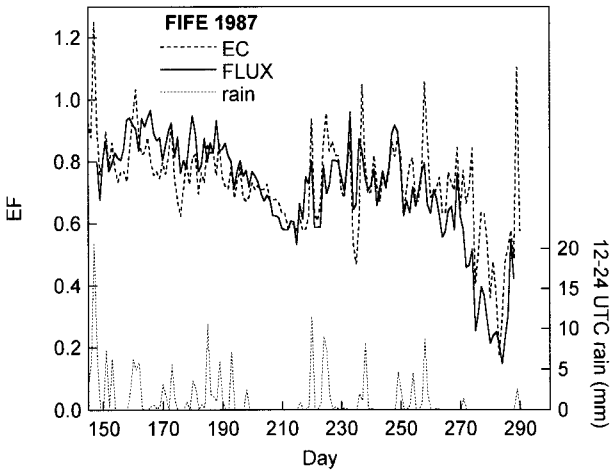

FIG. 6. Comparison of daytime evaporative fraction (upper curves), with model precipitation below (right-hand scale).

b. Sensible and latent heat fluxes

Figure 5 compares the daytime (1200–2400 UTC average) surface latent (LH) and sensible heat (SH) fluxes for the season. On the whole, the ability of the model to track the observed variation of the surface fluxes is very good. Evaporation stays a little high in the fall relative to the data, but this is not very surprising as the model has no seasonal cycle of vegetation (see later). It is noticeable that the model drop in LH flux is generally less than the data on most days when the data has a sharp fall, because of cloud or rain. Figure 6 shows daytime evaporative fraction [EF = LH/(LH + SH)]. The model tracks the observations quite well seasonally, although it is biased low in spring and high in fall. However, there are notable model peaks on many days, when it rains in the model (lower curve on right-hand scale). The reevaporation off the wet canopy in the model may be too high (or the data may suffer from some low bias on wetter days).

c. Comparison of soil moisture profiles and rainfall

The EC model carries soil moisture as a variable for four layers—0–7, 7–28, 28–100 cm, and a base layer of 100–289 cm. The first three contain the rooting zone (Viterbo and Beljaars 1995). We calculated mean values for equivalent soil layers from the site-averaged gravimetric and neutron probe soil moisture data (see Betts and Ball 1998). Figures 7a,b show the comparison for the season. The upper curves in Fig. 7a are the four EC model layers, showing the impact of the major rainfall events in the model (on right-hand scale) on soil moisture. The large rainfall events bring the four soil layers to 30%–35% water by volume. During the dry spells, particularly late July, the upper three layers dry out, and the upper layer falls to 16% soil moisture by 3 August, when the first rain falls after two dry weeks. The response to rainfall events, and the dry-downs between them, seem satisfactory, as shown in Viterbo and Beljaars (1995) in off-line tests, although we will comment on the impact of soil moisture nudging in the model below.

Figure 7b is the corresponding set of graphs for the FIFE site average of soil moisture and rainfall. The general pattern is similar, although there are many differences. The observed intense rainfall events on days 148 and 225 had more precipitation than in the model; not too surprising, perhaps, as the model is representative of a larger grid square of order 100 km, while the FIFE site is only 15 km × 15 km. The deep soil moisture (for the 100–200-cm depth layer) at the FIFE site had a value around 33%, slightly higher than in the

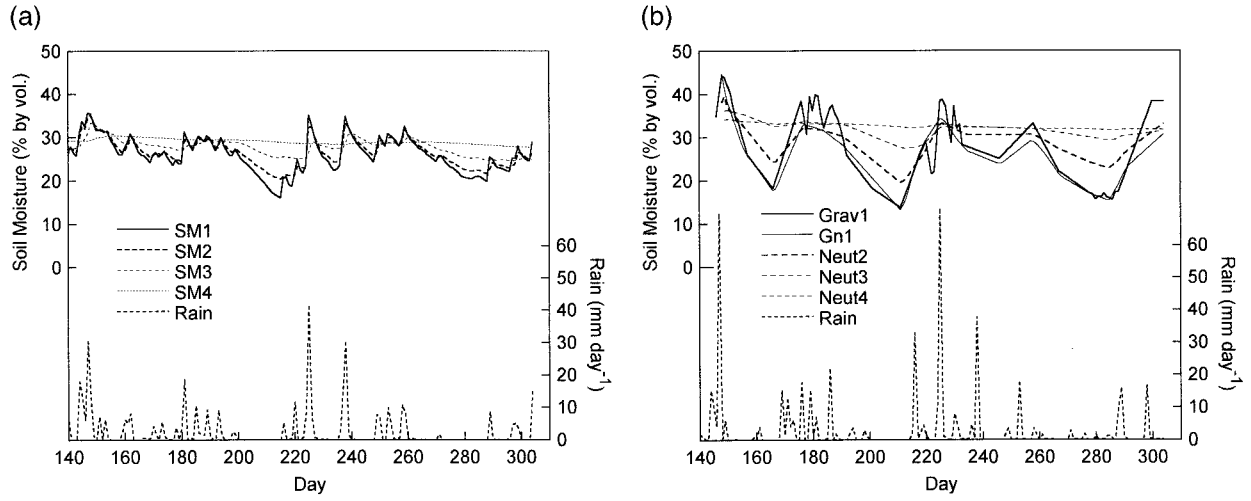

FIG. 7. (a) The 24-h average volumetric soil moisture and daily precipitation for the four soil layers in the ECMWF model for the 1987 season. (b) As in (a) but for corresponding layers for FIFE soil moisture. Two curves are shown for upper 0–7-cm layer with different time sampling (see text).

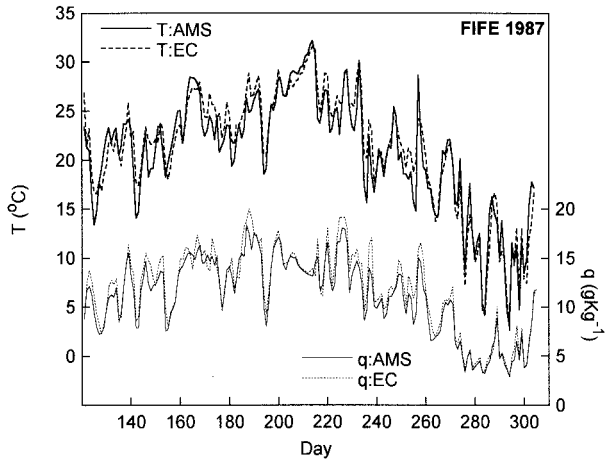

FIG. 8. As in Fig. 1 but for 2-m temperature T and mixing ratio q. Data is AMS site average.

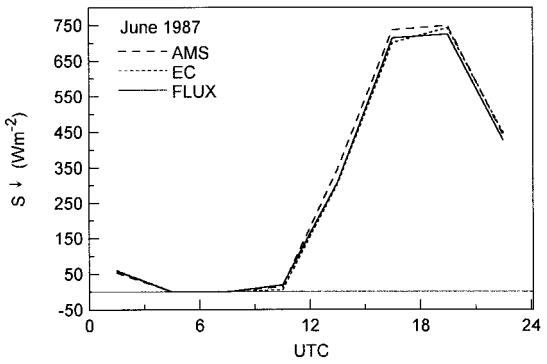

FIG. 9. Comparison of mean June diurnal cycle of incoming solar radiation S↓ Data is AMS and FLUX averages.

model. In general, the amplitude of the fall in soil moisture by volume for the surface (0–7 cm) layer is larger in the data than the model. We show two curves for this level: the heavy solid line is for all the gravimetric sites (converted to a volumetric value), while the light solid line is for that subset of samples near and at the times of the neutron probe data [which are in a merged neutron probe data file in Strebel et al. (1994)]. Irregular time sampling is a problem with the FIFE soil moisture data. During the four IFCs, almost daily gravimetric measurements were made, as can be seen from the high-frequency fluctuations with rainfall events for the upper layer. However, the neutron probe sites were sampled less frequently, so the corresponding curves are smoother. Between IFCs, sampling was least frequent, and as a result, some rainfall events, such as on day 238, were not seen at all by the soil moisture data. This sampling problem must be borne in mind in comparing Figs. 7a, and 7b. The data corresponding to the second model level (7–28 cm) are the poorest, since the neutron probe data at 20 cm is not reliable (see appendix in Betts and Ball 1998), and we have simply averaged the gravimetric data at 7.5 cm (converted to volumetric soil moisture) and the 30-cm neutron probe data. The trough in observed soil moisture on day 166 in June is somewhat puzzling. There are measurements on this one day, but the model (which admittedly shows more precipitation than the data during this dry June spell) has no correspondingly low value, and, curiously enough, the observed evaporation remains high through this period.

Our main conclusion is that the EC model is reproducing the main features of the seasonal soil moisture behavior but with reduced amplitude in the near-surface layers. The model was developed using this same FIFE data (Viterbo and Beljaars 1995), and when we compare with Fig. 9 of that paper, we see that the amplitude in the reanalysis model is a little less than in the off-line simulation. The probable reason is that the subsequent addition of soil moisture nudging to the model (Viterbo and Courtier 1995) has ''added'' some soil moisture during extended dry periods. For the 10 dry days 205–214 (see section 4d), the loss of water due to evaporation is 4.35 cm (126 W m^{-2} for 10 days), while soil moisture in the first three layers falls only 3.33 cm, considerably reduced, because nudging adds 0.80 cm of water to the same three layers. The small imbalance is diffusion from the base layer.

d. Seasonal variation of temperature and mixing ratio

Figure 8 shows the 24-h average 2-m temperature T and mixing ratio q for model and data for the season. The biases in the daily mean are small; typically the model is a little warmer (by 0.4 K in the mean) and wetter (by 0.7 g kg^{-1} in the mean) than the data. The biases are larger (not shown) for the 12-h daytime (1200–2400 UTC) average (+1.6 K and 0.8 g kg^{-1}), while at night, the model is cooler (−0.7 K) but still wetter (+0.7 g kg^{-1}). These model errors are much reduced over our earlier study (Betts et al. 1993). Because there is a small north to south climatological gradient of soil moisture (0.5 g kg^{-1} per degree of latitude in the ECMWF reanalysis in summer), the actual model bias of humidity is probably only +0.5 g kg^{-1}, as the FIFE data is about 1/3° north of the model grid point. We show the diurnal cycle in the next section.

e. Mean diurnal cycle in different seasons

The previous figures show the seasonal cycle and some day–night differences. We now give some comparisons of the mean diurnal cycle in different seasons. Figure 9 shows the June-average comparison of incoming solar radiation $S\downarrow$. We show two data curves: the average for the AMS sites and a second for the FLUX sites, to give some estimate of the uncertainty in the data. The reanalysis model, with the prognostic cloud scheme (Tiedtke 1993) and the current radiation scheme, has no detectable mean error: a huge improvement on

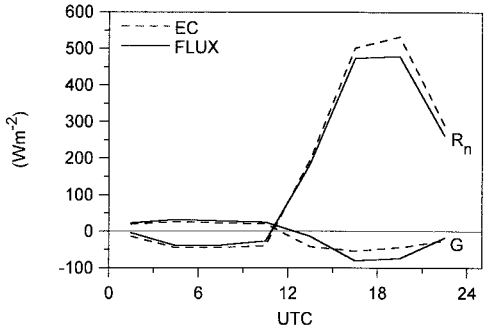

FIG. 10. As in Fig. 9 but for net radiation and ground heat flux; data is FLUX average.

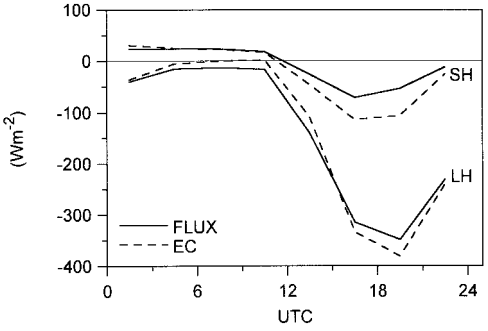

FIG. 11. As in Fig. 10 but for surface sensible and latent heat fluxes.

earlier model versions, as mentioned earlier, and on some other forecast models (Betts et al. 1996; Betts et al. 1997). Other months show similar mean comparisons (not shown). Figure 10 shows a June-mean diurnal cycle of net radiation R_n and ground flux G. The amplitude of the model diurnal cycle of G appears a little low and that of R_n a little high. However, the daytime model bias in R_n of about $+40$ W m^{-2} (about 8%) is not consistent with the lack of bias in the incoming solar radiation despite the lower albedo in the model. Some of this R_n bias probably comes from the uncertainty in the calibration of the FIFE net radiation instruments (Smith et al. 1992a; Smith et al. 1992b). The ground heat flux may show a real model bias, as it changes sign during the season (see below), although the absolute value of the FIFE ground flux values depend on the site locations from year to year (Betts and Ball 1998), as discussed earlier. Figure 11 shows the SH and LH flux comparison for June. In the daytime, both model SH and LH fluxes are high ($R_n - G$ is high), and the model EF is low (as in Fig. 6). Figure 12 compares the June diurnal cycle of 2-m T and q. Three curves are shown for each: the FIFE AMS data (solid), the EC reanalysis every 6 h (dashed), and the 3-h EC values from each 0–6-h forecast from each reanalysis (dotted). The model diurnal cycle of temperature is too large. The model is cooler at sunrise, which we will discuss later in section 4, and warmer during the daytime than the data, which is consistent with the larger sensible heat flux shown in Fig. 11. For mixing ratio, the model analysis is on average a little moister than the FIFE data, and the model short-term 0–6-h forecasts show a strong midmorning peak in q (at 1500 UTC), followed by a fall to a drier value than the FIFE data at 2400 UTC in late afternoon. This diurnal cycle of mixing ratio in the model, which is very different than the data, is a characteristic of the EC reanalysis model and has important consequences, which will be discussed further in section 4b. Note that at 2400 UTC, the model 6-h forecast is significantly drier than the EC reanalysis, so that the soil moisture nudging increment at this analysis time is positive (see section 4d later).

Although we do not show every month, the biases between model and data have a steady trend through July, August, and September. The small positive bias in daytime net radiation continues (but we doubt if it is real, because of the calibration uncertainties in the FIFE data mentioned above), but the initially small model diurnal cycle in G gets larger relative to the data, until by September and October, the model diurnal cycle of G is greater than that observed. We have commented on this earlier in Fig. 4. In fact, the seasonal change of the model diurnal cycle of G, shown in Fig. 13a, is almost the reverse of that observed (Fig. 13b). At night, the model G increases from May to October, while the daytime changes of G in the model are small. In the FIFE data, G decreases slightly at night and strongly during the daytime from June to October. (No average for May is shown and the October average is only for 1–16 October.) This model difference in G needs further study, as it impacts the seasonal cycle of soil temperature in the model (not shown). One factor, which is not represented in the model, is the dependence of soil heat flux on soil moisture, which is significant in the data (Betts and Ball 1998).

Figure 14 shows the mean diurnal cycle of SH and LH fluxes for 12 sunny days in the first half of October (1–9 and 11–13 October). At night, observations and model SH flux agree well, but in the daytime, the model SH is low and LH high, so that the bias in model EF

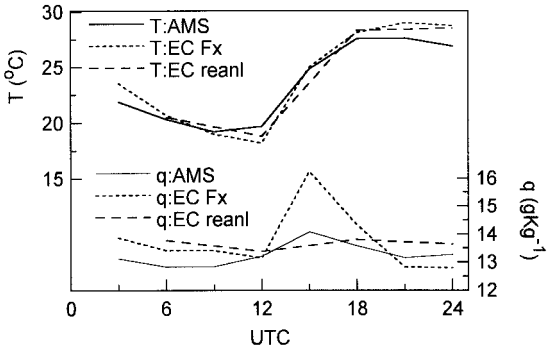

FIG. 12. As in Fig. 10 but for 2-m temperature and mixing ratio; data is AMS average; model is EC reanalysis and short-term 0–6-h forecasts.

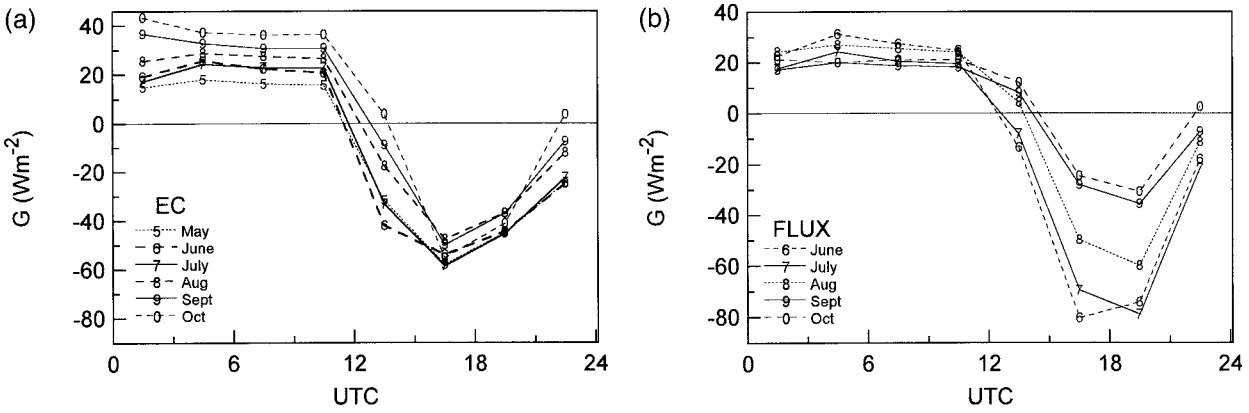

FIG. 13. (a) Diurnal cycle of ground heat flux in the model from May to October. (b) Diurnal cycle of ground heat flux in the FIFE data from June to October.

has changed sign from negative (in June) to positive in October. This seasonal shift of model Bowen ratio from too little evaporation in spring to too much in fall is probably because the model has no seasonal cycle of vegetation. In October, the FIFE grassland has reached senescence, after the first hard frost (1 October), and evaporation is low. Figure 15 shows the corresponding mean diurnal cycle of T and q for these 12 days in October for the analysis, the short-term forecasts, and the AMS data. The model morning T minimum is low by 2.5 K (larger than in June), but in contrast to June, when the model was warm, the afternoon temperature maximum in the model is now a little cool, presumably because the model SH flux is now low. Most of the day, the model is moister than the data, consistent with its larger LH flux.

4. Comparison during July dry-down

a. Time sequence of low-level variables

The period from Julian day 205 to 215 (24 July–2 August 1987) is of interest because there was no rain in either the model or the FIFE data. We will use it to explore further the characteristics of the model diurnal cycle. Figure 16 shows the sequence of temperature T and mixing ratio q (lower curves) at a 3-h time resolution. The time axis is a decimal Julian day. The daily maximum temperatures steadily rise as the soil dries, and the surface EF falls (not shown). The reanalysis short-term forecast tracks the 2-m daytime temperature maximum very well, but the model T minimum is typically low by 3 K (as in Fig. 12). The mixing ratio comparison shows two anomalies in the model, although the mean mixing ratio is approximately correct. There is a midmorning (1500 UTC) peak of q in the model every day, and an evening (2400 UTC) q minimum (which is generally greater than the minimum observed). We also saw these features in the June average (Fig. 12). Figure 17 shows two important consequences. There is a larger diurnal range in model P_{LCL} (the pressure height of the lifting condensation level above the surface): closer to saturation at sunrise and a higher value (a lower relative humidity) at sunset. There is also a larger diurnal amplitude of model θ_e (equivalent potential temperature), with a peak in midmorning, which is often 5 K more than the data, and a corresponding low θ_e minimum near sunset. Since low-level θ_e and P_{LCL} are the primary controls on moist convection, these model anomalies, if widespread, would favor enhanced late morning convection and suppressed evening convection. This is consistent with operational experience of precipitation biases in summer ECMWF forecasts. We also see this in Fig. 18, which compares the diurnal

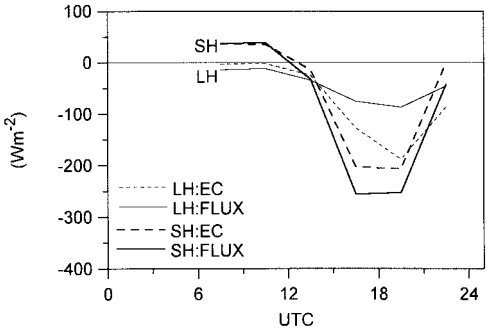

FIG. 14. As in Fig. 11 but for average of 1–9 and 11–13 October.

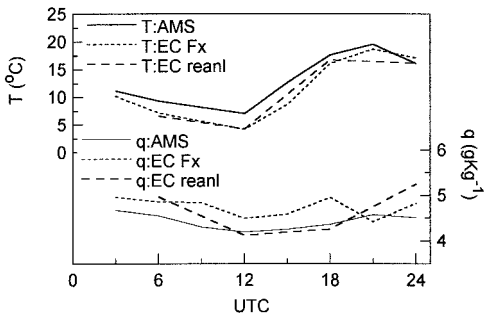

FIG. 15. As in Fig. 12 but for average of 1–9 and 11–13 October.

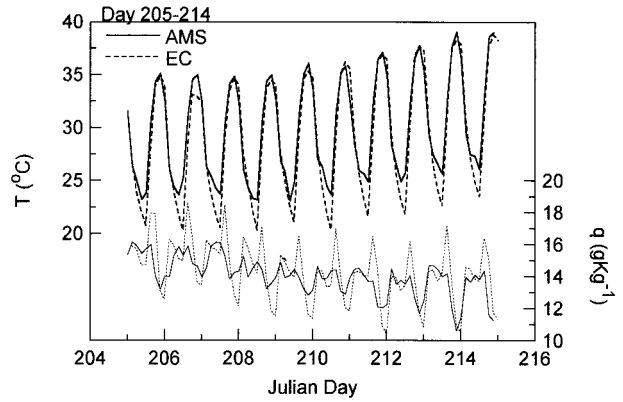

FIG. 16. Comparison of 2-m temperature and mixing ratio for late July dry-down: Julian days 205–214.

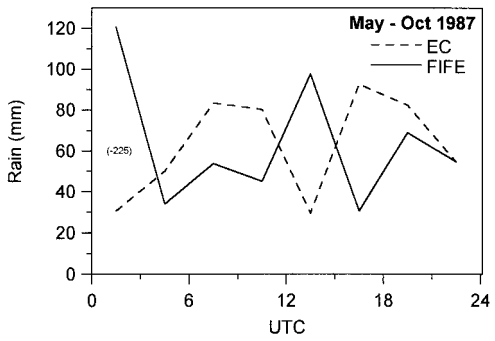

FIG. 18. Comparison of the diurnal cycle of precipitation for period May–October 1987. The point (−225) is discussed in the text.

cycle of precipitation for the FIFE point for model and data, summed in 3-h bins for the months May–October. The total precipitation is almost identical for both (505 mm). Both model and data also show double peaks, but at different times. The EC model has a peak for the time period 1500–1800 UTC, immediately following the midmorning θ_e peak in Fig. 17, and a sharp minimum following sunrise, when the model has a cold bias. In contrast, the FIFE data has peaks just after sunrise and sunset, and a *minimum* for the 1500–1800 UTC interval. The FIFE peak for 0000–0300 UTC is strongly determined by the largest rainstorm of the summer on day 225, when nearly 60 mm of rain fell in this one time interval. If this one day is excluded from the summer's average, the FIFE sum for this time interval drops [to the point marked (−225)] slightly below the FIFE afternoon peak, but the comparison is otherwise almost unchanged.

b. 10-day mean diurnal sequence

The next few graphs show the 10-day mean diurnal average for days 205–214. Figure 19 shows the *T* (upper and left-hand scale) and *q* comparison (lower and right-hand scale). There are again two model plots: the one at 3-h time resolution corresponds to the average of Fig. 16, constructed from the 3–6-h short-term forecast from each analysis; the one at 6-h time resolution is the model analysis itself. For *T*, the two model diurnal sequences are close; the low bias in temperature of the model at 1200 UTC (near sunrise) is visible, and at 2400 UTC (near sunset) the model has a small high *T* bias. The *q* comparison shows the large midmorning model peak in the short-term *q* forecast at 1500 UTC (this is not an analysis time). The model analysis and 6-h forecast agree at 1200 UTC, but at 2400 UTC there is the interesting and puzzling result that the analysis is wetter than the data, but the 6-h forecast for this time, as we have seen earlier, is much drier (by about 2 g kg^{-1}). The data show a small diurnal cycle with a fall of *q* in the afternoon; the analysis shows almost no diurnal cycle (at 6-h resolution), while the short-term model forecast has the much-too-large diurnal cycle seen in Fig. 16. This is important, because the reanalysis model uses the difference between the 6-h forecast of *q* and the analysis to nudge soil moisture.

The bias in net radiation is rather small for this 10-day average (not shown). However, in the morning, the model LH flux is smaller than observed, and in the late afternoon the model is larger, with the reverse behavior

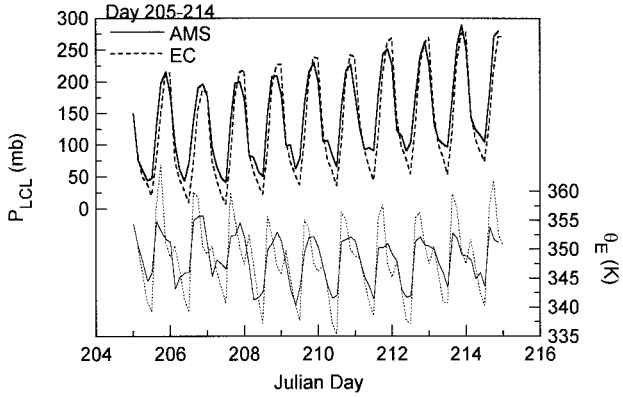

FIG. 17. As in Fig. 16 but for pressure height of lifting condensation level P_{LCL} and equivalent potential temperature θ_e.

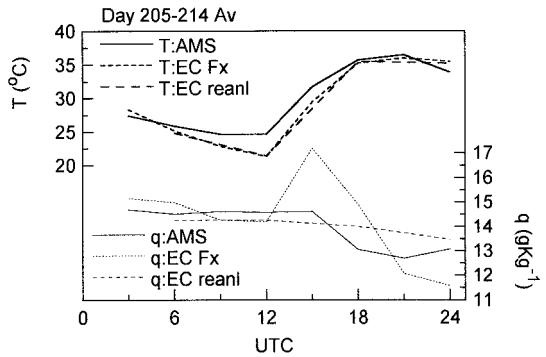

FIG. 19. As in Fig. 12 but for 10-day average (Julian days 205–214).

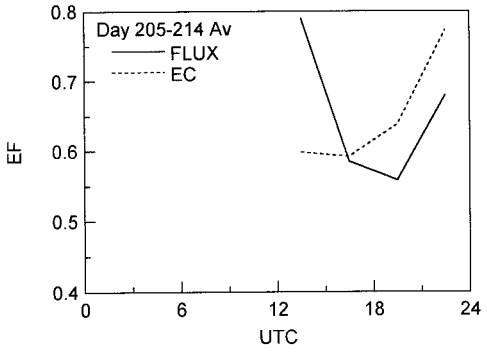

FIG. 20. As in Fig. 20 but for daytime evaporative fraction (Julian days 205–214).

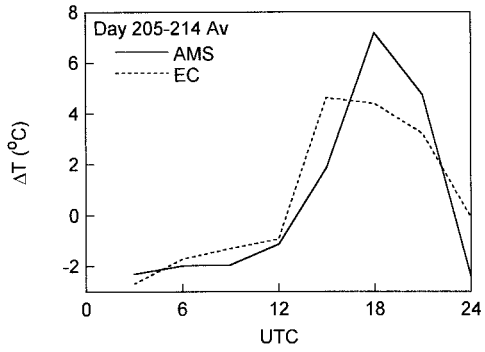

FIG. 21. As in Fig. 20 but for $\Delta T = T_{sfc} - T_2$.

for the sensible heat (not shown). Figure 20 compares the daytime EF, showing this rather different model diurnal behavior from the observations. It is clear that the model surface evaporation is not the cause of the model q biases in Fig. 16, since in the morning the model q spike at 1500 UTC follows *low* model evaporation relative to the data, and the low model q at 2400 UTC follows *high* model evaporation. This means that these model q anomalies in the diurnal cycle must be related to the BL depth, which controls the depth of the vertical mixing of the surface evaporation. The BL must be too shallow in the morning because of the too-cold minimum surface temperature at sunrise, which is associated with a stronger model surface inversion. We will explicitly check this in the next section. In the evening, the only explanation for the opposite trends in q for model and data between 2100 and 2400 UTC must be that the deep model BL remains fully coupled, while the FIFE BL starts to decouple sooner. A possible clue to this evening difference is shown in Fig. 21 for the mean temperature difference $\Delta T = T_{sfc} - T_2$. The observed T_{sfc} is a measured radiometric temperature, not an aerodynamic temperature, while in the model these are not distinguished. The model uses a smaller roughness length for heat than momentum as observed (Betts and Beljaars 1993). In the morning, the model ΔT is larger than observed, qualitatively consistent with the larger SH flux, while in the late afternoon the observed ΔT plunges, as the radiometric T_{sfc} falls much faster than the model temperature (not shown).

This leaves two questions: why is the model too cool at sunrise at the surface, and why does the model T_{sfc} not fall faster near sunset? The first may be related partly to the stable BL parameterization (Viterbo et al. 1997), but there appear also to be important differences in the incoming longwave between model and data shown in Fig. 22. The model has a larger diurnal amplitude in LW↓ than the FLUX data, with the result at night that the model LW↓ is 20 W m^{-2} lower than observed. This is one likely cause of the fall of model T_{sfc} to a mean value 3 K lower than observed at 1200 UTC (giving a net outgoing LW flux in the model that is only about 10 W m^{-2} greater than observed). A possible cause of this model LW↓ bias might be an underestimate of cloud cover at night, but the larger model daytime value also asks for an explanation. We have no explanation for the slower fall of the model T_{sfc} in late afternoon.

c. Sensitivity to the stable BL parameterization

Recently, changes to the stable BL parameterization have been tested at ECMWF (Viterbo et al. 1997) to reduce the cold bias of the model at night, by increasing the coupling of the land surface to both the stable BL above and to the ground below. One important effect of this change is to weaken the nocturnal inversion at sunrise, and this in turn affects the BL development in the morning, reducing the midmorning peak in q. Figure 23 shows three curves of the diurnal cycle (at hourly resolution) for a 2-day average (from 0000 UTC on day 209 to 0000 UTC on day 211). The solid line is the FIFE AMS data at 2 m. The dotted and heavy dashed lines are for the lowest model level (level 31 at about 30 m above the surface) extracted from two 120-h forecasts initialized at 1200 UTC on day 208 (27 July 1987), one a control using a model with the same land physics as the reanalysis model, and the second with the new stable BL and ground flux scheme (heavy dashes). The control shows the same midmorning peak at 1500 UTC, followed by a much steeper fall than the data to a low

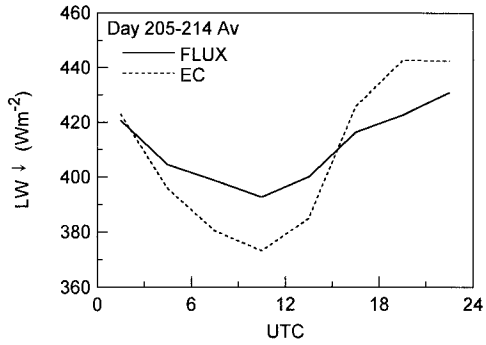

FIG. 22. As in Fig. 20 but for incoming longwave radiation (LW↓).

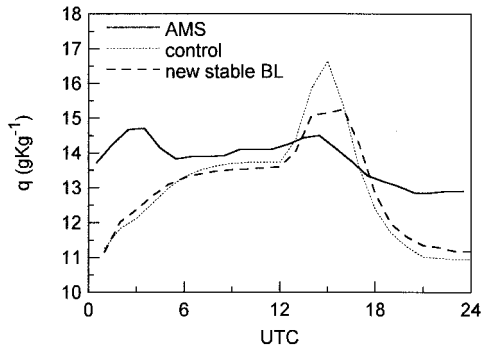

FIG. 23. Diurnal cycle of mixing ratio for 2-day average (209–210), showing FIFE AMS data (at 2 m), reanalysis land physics (control), and revised stable BL scheme at lowest model level 31.

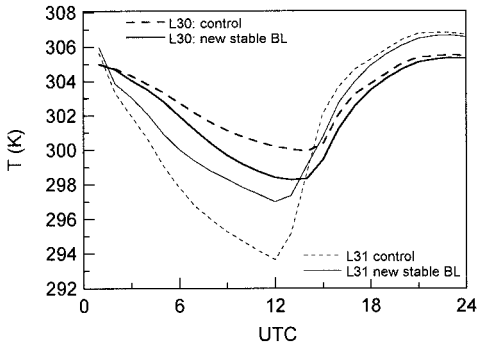

FIG. 24. Two-day average diurnal cycle of temperature at two lowest model levels for two model versions.

afternoon value, as in Fig. 19. For the forecast with the new stable BL scheme, the midmorning peak of q is sharply truncated, a significant improvement, as the BL deepens sooner to the next model level (30, not shown). The reason is that there is a significant difference in the stability near the surface at sunrise. Figure 24 shows the corresponding average diurnal cycle of temperature for the two model versions at level 31 and the next level 30 (about 150 m above the surface). Whereas the model with the improved stable BL is more than 3 K *warmer* near sunrise at L31, it is 1.5 K *cooler* at L30. Consequently as the lowest level 31 warms after sunrise, it starts mixing upward to the next level 30 much sooner that in the reanalysis control model. This upward mixing sharply truncates the morning rise of q, as seen in Fig. 23. This new stable BL scheme was implemented in the operational model on 19 September 1996, together with a parameterization of soil freezing (Viterbo et al. 1997). Note that the sharp fall of q in the model near local noon is not reduced much, and the late afternoon low bias is only slightly improved, as the afternoon BL is a little shallower (not shown). This shallower BL is a consequence of the new surface scheme (which has a larger ground heat flux) having a reduced surface SH flux (not shown), so that the low-level afternoon temperature is a little lower in the new surface model, as shown in Fig. 24.

d. Impact of nudging for days 205–214

Figure 25 shows the 10-day mean diurnal cycle of volumetric soil moisture for the three upper model layers for the analysis (dotted) and the model 0–6-h forecasts (solid). The small difference between the curves is the nudging increment at the analysis times. It is the same for all three soil layers and is directly proportional to the q analysis increment in Fig. 19. The total addition of soil moisture to the top three layers (1-m depth) in a 6-h interval (Δt) is given by

$$\Delta(\mathrm{SM}) = C_v D \Delta t (q_a - q_g), \qquad (2)$$

where C_v is the vegetation fraction (included so that there is no nudging over deserts). In the reanalysis model, the coefficient D is set so that, if the moisture analysis increment $(q_a - q_g) = 3$ g kg^{-1}, then 0.15 m of water is added to the soil in 12 days (the operational model uses a higher rate of nudging; the corresponding timescale is 4.5 days). The nudging is also constrained so that the field capacity and the permanent wilting point thresholds are never crossed (by the nudging).

The nudging increment is negative at 0600 UTC, and larger positive at 2400 UTC. Over the 10-day period, 8 mm of water are added to the soil by nudging. The model evaporates 3.6 mm more than observed for the time period. (It should be noted that the flux average is of relatively poorer quality during this time period than during the intensive field campaigns.) It appears that the model dry-down in late afternoon seen in Figs. 16 and 19 leads to a significant net addition of soil moisture by nudging and a small net positive bias in both evaporation (+10 W m^{-2}) and mixing ratio (+0.3 g kg^{-1}). The comparison of the diurnal cycle of q for the 3-month average for June–August 1987 (not shown) is qualitatively similar to those in Figs. 12 (for June) and Fig. 19 for the dry period. In the mean, a large positive nudging increment comes from the afternoon dry-down of the model short-term forecasts (which is also clearly

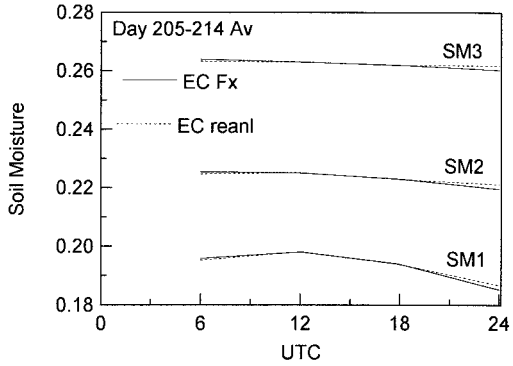

FIG. 25. Ten-day mean (day 205–214) of diurnal cycle of three upper soil layers in the EC model, showing analysis (dashed) and short-term forecast (solid). Difference is the nudging.

seen in the forecasts shown in Fig. 23). It is possible that the moist bias seen in Fig. 8 during much of the summer comes largely from this excessive afternoon nudging of soil moisture. In the 3-month June–August average, the EC analysis is on average 0.8 g kg^{-1} moister than the data, of which perhaps 0.2 g kg^{-1} may again be due to the north–south climatological humidity gradient between the FIFE data and the model grid point.

5. Conclusions

Data from the FIFE experiment for the summer season of 1987 are used to assess the land-surface interaction of the ECMWF reanalysis. In comparison with an earlier study (Betts et al. 1993) using the 1992 ECMWF operational model, the land-surface interaction is greatly improved, following several recent model changes: a new four-layer prognostic soil model (Viterbo and Beljaars 1995), the addition of prognostic clouds (Tiedtke 1993), and the nudging of soil moisture using q analysis errors (Viterbo and Courtier 1995). The previous high bias in the incoming solar radiation has been removed (the reintroduction of climatological aerosols being partly responsible here). The summer daytime temperature maxima agree well with the data, but under clear skies the model has too low a morning temperature minimum, which is discussed further below.

The four-layer soil moisture model depicts the seasonal cycle well, and the root zone is recharged satisfactorily after major rain events. Consequently, the evaporative fraction over the season is now generally quite good, much better than in Betts et al. (1993). In June, the EF in the model is a little low, but later in the summer, and particularly the fall, there is a tendency for model evaporation to be higher than observed. One reason is the absence of a seasonal cycle in the model vegetation, but during the summer, it appears that it may be partly an impact of the soil moisture nudging, which is positive. As a result, mean mixing ratio is a little higher than observed. Evaporative fraction also appears too high in the model just after rainfall.

In spring, the diurnal ground heat flux amplitude is underestimated a little, and the near-surface soil temperatures appear to be consequently low (not shown). In the fall, the ground heat flux amplitude is too large, so it appears that the model lacks a seasonal control on the soil heat flux, perhaps the dependence of thermal conductivity on soil moisture.

We studied a 10-day dry period (24 July–2 August) in some detail to explore two noticeable errors in the surface diurnal thermodynamic cycle. The temperature minimum at sunrise is low by several degrees, because the surface uncouples too much at night under the stable boundary layer. It appears that a low bias in the incoming longwave radiation at night is an important contribution to this, although the minimum temperature bias can be reduced greatly by changes to the stable BL scheme (Viterbo et al. 1997), implemented on 19 September 1996 in the operational model. There is also an unrealistic diurnal cycle of mixing ratio q, which may feed back on the diurnal cycle of precipitation. The model has a characteristic sharp midmorning peak of mixing ratio, which is related to a too-shallow BL following the low morning T minimum, which slows the deepening of the boundary layer. Before sunset, the observed mixing ratio typically rises, while the model forecast mixing ratio falls sharply after its early morning rise and stays low. This late afternoon (at 2400 UTC at the FIFE site) minimum of mixing ratio (below that of the analysis) leads to large positive nudging of soil moisture in the analysis cycle. We see this both for this 10-day dry period, as well as for the whole June–August period. Thus, it appears that a bias in the model in the late afternoon q feeds back on the diurnally averaged nudging increment in a systematic way. This may be responsible for the slight moist bias (of 0.5 g kg^{-1} for the summer, if we correct for the north–south climatological gradient across Kansas and the north–south separation of the model grid point and the FIFE data) and for the slightly high LH flux in the model. We speculate that the uncoupling of the model BL from the surface in the evening is later than observed, but this needs further study. One impact of this net positive nudging of soil moisture appears to be that the amplitude of the soil moisture variations in the model are damped, compared to an earlier off-line study (Viterbo and Beljaars 1995) and the FIFE observations (Betts and Ball 1998).

While the overall comparison is encouraging and represents significant progress since our earlier study (Betts et al. 1993), we have identified several areas where further model development would be desirable. Attention needs to be given to possible biases in the longwave radiation code, which affect the nighttime skin temperature. Seasonal EF in the model could probably be improved by the addition of a seasonal cycle of vegetation. An improved seasonal dependence in the ground storage is desirable, as it affects the seasonal cycle of ground temperature. The cause of the erroneous model diurnal cycle of mixing ratio needs further study, as it feeds back both on the nudging of soil moisture and probably the diurnal cycle of convection and precipitation. Improvements are needed in the modeling of the diurnal evolution of the boundary layer.

Acknowledgments. Alan Betts acknowledges support from the National Science Foundation under Grant ATM-9505018, NASA under Contract NAS5-32356 for the processing of the FIFE data, and ECMWF for travel support.

REFERENCES

Beljaars, A. C. M., P. Viterbo, M. J. Miller, and A. K. Betts, 1996: The anomalous rainfall over the United States during July 1993:

Sensitivity to land surface parameterization and soil moisture anomalies. *Mon. Wea. Rev.*, **124,** 362–383.
Bengtsson, L., and J. Shukla, 1988: Integration of space and in situ observations to study global climate change. *Bull. Amer. Meteor. Soc.*, **69,** 1130–1143.
Betts, A. K., and J. H. Ball, 1995: The FIFE surface diurnal cycle climate. *J. Geophys. Res.*, **100,** 25 679–25 693.
——, and ——, 1998: FIFE surface climate and site-average dataset 1987–89. *J. Atmos. Sci.*, in press.
——, and A. C. M. Beljaars, 1993: Estimation of roughness length for heat and momentum from FIFE data. *Atmos. Res.*, **30,** 251–261.
——, J. H. Ball, and A. C. M. Beljaars, 1993: Comparison between the land surface response of the European Centre model and the FIFE-1987 data. *Quart. J. Roy. Meteor. Soc.*, **119,** 975–1001.
——, S.-Y. Hong, and H.-L. Pan, 1996: Comparison of the NCEP/NCAR reanalysis with 1987 FIFE data. *Mon. Wea. Rev.*, **124,** 1480–1498.
——, F. Chen, K. E. Mitchell, and Z. I. Janjić, 1997: Assessment of land surface and boundary layer models in two operational versions of the NCEP Eta Model using FIFE data. *Mon. Wea. Rev.*, **125,** 2896–2916.
Gibson, J. K., P. Kallberg, S. Uppala, A. Hernandez, A. Nomura, and E. Serrano, 1997: ERA description. ECWMF Re-Analysis Project Rep. Series 1, ECMWF, Reading, United Kingdom, 72 pp.
Kalnay, E., and Coauthors, 1996: The NCEP/NCAR 40-year reanalysis project. *Bull. Amer. Meteor. Soc.*, **77,** 437–471.
Lott, F., and M. J. Miller, 1997: A new sub-grid scale orographic drag parametrization: Its formulation and testing. *Quart. J. Roy. Meteor. Soc.*, **123,** 101–127.
Morcrette, J.-J., 1990: Impact of changes in the radiative transfer parameterization plus cloud optical properties in the ECMWF model. *Mon. Wea. Rev.*, **118,** 847–873.
Richie, H., C. Temperton, A. J. Simmons, M. Hortal, T. Davies, D. Dent, and M. Hamrud, 1995: Implementation of the semi-Lagrangian method in a high-resolution version of the ECMWF forecast model. *Mon. Wea. Rev.*, **123,** 489–514.
Schubert, S. D., R. B. Rood, and J. Pfaendtner, 1993: An assimilated dataset for earth science applications. *Bull. Amer. Meteor. Soc.*, **74,** 2331–2342.
Sellers, P. J., and F. G. Hall, 1992: FIFE in 1992: Results, scientific gains, and future research directions. *J. Geophys. Res.*, **97,** 19 091–19 109.
——, F. G. Hall, G. Asrar, D. E. Strebel, and R. E. Murphy, 1988: The First ISLSCP Field Experiment (FIFE). *Bull. Amer. Meteor. Soc.*, **69,** 22–27.
Simmons, A. J., and R. Strüfing, 1981: An energy and angular momentum conserving scheme, hybrid coordinates and medium-range weather prediction. ECMWF Tech. Rep. 28, Reading, United Kingdom, 68 pp.
Smith, E. A., W. L. Crosson, and B. D. Tanner, 1992a: Estimation of surface heat and moisture fluxes over a prairie grassland, 1. In situ energy budget measurements incorporating a cooled mirror dew point hygrometer. *J. Geophys. Res.*, **97,** 18 557–18 582.
——, and Coauthors, 1992b: Area-averaged surface fluxes and their time-space variability over the FIFE experimental domain. *J. Geophys. Res.*, **97,** 18 599–18 622.
Strebel, D. E., D. R. Landis, K. F. Huemmrich, and B. W. Meeson, 1994: Collected data of the First ISLSCP Field Experiment. *Surface Observations and Non-Image Data Sets*, Vol. 1, NASA/Goddard Space Flight Center, CD-ROM. [Available from NASA/Goddard Space Flight Center, Greenbelt, MD 20771.]
Tanre, D., J.-F. Geleyn, and J. M. Slingo, 1984: First results of the introduction of an advanced aerosol-radiation interaction in the ECMWF low resolution global model. *Aerosols and Their Climate Effects*, H. E. Gerber and A. Deepak, Eds., A. Deepak, 133–147.
Tiedtke, M., 1989: A comprehensive mass flux scheme for cumulus parameterization in large-scale models. *Mon. Wea. Rev.*, **117,** 1779–1800.
——, 1993: Representation of clouds in large-scale models. *Mon. Wea. Rev.*, **121,** 3040–3061.
Viterbo, P., and A. C. M. Beljaars, 1995: A new land surface parameterization scheme in the ECMWF model and its validation. *J. Climate*, **8,** 2716–2748.
——, and P. Courtier, 1995: The importance of soil water for medium-range weather forecasting. Implications for data assimilation. *Workshop on Imbalance of Slowly Varying Components of Predictable Atmospheric Motions*, Beijing, China, World Meteor. Org., 121–130.
——, A. C. M. Beljaars, J.-F. Mahfouf, and J. Teixeira, 1997: The role of soil water freezing and its interaction with the stable boundary layer. Research Activities in Atmospheric and Oceanic Modeling, CAS/JSC Working Group on Numerical Experimentation Rep. 25, WMO/TD-No. 792, Geneva, Switzerland, 4.44–4.45.